Journal of Drug Delivery Science and Technology 88 (2023) 104898

Contents lists available at ScienceDirect

Journal of Drug Delivery Science and Technology

journal homepage: www.elsevier.com/locate/jddst

# Formulation and *in vitro* skin diffusion of colchicine using different drug delivery vehicles

Micaela Ponte, Wilna Liebenberg, Minja Gerber *

*Centre of Excellence for Pharmaceutical Sciences (Pharmacen™), North-West University, Private Bag X6001, Potchefstroom, 2520, South Africa*

## 1. Introduction

Historically known as "the disease of kings," gout is one of the oldest known types of arthritis, affecting more than 40 million people worldwide, prevalent in patients between 30 and 50 years of age, and frequently experienced more by males than females [1–4]. It is a result of monosodium urate crystal deposition in tissues (cartilage and joints), consequently causing an immune response [5–7]. Clinical manifestations include severe pain and inflammatory attacks affecting common joints, chronic joint damage and tophaceous deposits of monosodium urate crystals in the skin and joints [1,4]. Gout is an understood and manageable rheumatic disease, the treatment of which is mostly non-steroidal anti-inflammatory drugs (NSAIDs, i.e., indomethacin and naproxen) due to their efficacy and low toxicity when administered orally [7,8]. Furthermore, there are three different active pharmaceutical ingredients (APIs) used for the treatment of gout, each having different mechanisms of action, which includes allopurinol: an API that inhibits uric acid production, probenecid: an API that increases uric acid excretion and finally, colchicine: an API, which does not affect uric acid metabolism or elimination [9].

Colchicine is an API used in the treatment of acute gouty arthritis as well as prophylaxis for patients who experience reoccurring gout attacks [8]. Colchicine is an alkaloid that is isolated from *Colchicine autumnale* (autumn crocus), a plant that possesses anti-inflammatory properties [6]. When administered orally, colchicine, presents a decreased benefit-toxicity ratio, as it results in dose-dependent gastrointestinal adverse effects, such as nausea, vomiting, diarrhoea and abdominal pain in 50–80% of patients before achieving an outcome of gout relief [6,8]. Colchicine has a narrow therapeutic toxicity window and can be very toxic when used inappropriately, where gastrointestinal symptoms are usually the first feature of colchicine toxicity [7]. Due to colchicine's small therapeutic window, the transdermal delivery of colchicine may subsequently improve patient compliance through the relief of gout symptoms, while still avoiding any dose-dependent gastrointestinal adverse effects. This study will focus on the transdermal delivery of colchicine, which subsequently may improve patient compliance to relieve gout symptoms by avoiding any dose-dependent gastro-intestinal adverse effects.

## 2. Materials and methods

### 2.1. Materials

Colchicine came from DB Fine Chemicals (Sandton, South Africa). All formulated hydrogels, emulgels and nano-emulgels contained Carbopol® Ultrez 20, purchased from Lubrizol (Durban, South Africa). Each emulgel, nano-emulsion and nano-emulgel contained surfactants, Span® 60 (lipophilic surfactant) and Tween® 80 (hydrophilic surfactant) (both obtained from Sigma-Aldrich, Johannesburg, South Africa) and evening primrose oil (EPO) (Scatter Oils, Johannesburg, South Africa). The phosphate buffer solution (PBS; pH 7.4) was prepared with sodium hydroxide (NaOH) and potassium dihydrogen phosphate ($KH_2PO_4$), both purchased from Sigma-Aldrich (Johannesburg, South Africa). Throughout this study, ultrapure (UP) water was used and obtained from the Direct Pure® Ultrapure laboratory water purification system (Merck-Millipore, Midrand, South Africa). During each high-performance liquid chromatography (HPLC) experiment, there was chromatography grade acetonitrile and methanol used in addition to analytical grade formic acid, all purchased from Associated Chemical Enterprises (ACE) (Johannesburg, South Africa). Dow Corning® high vacuum grease, Whatman® filter paper and Parafilm® (obtained from Separations, Randburg, South Africa) were used during membrane release and skin diffusion studies. Dulbecco's Modified Eagle's Medium (DMEM) (purchased from HyClone, Separations, Johannesburg, South Africa), 1% non-essential amino acids (NEAAs), 1% penicillin/streptomycin (10000 U/ml) (both obtained from Lonza, Whitehead Scientific (Pty) Ltd, Cape Town, South Africa), 10% foetal bovine serum (FBS; Gibco, Thermo Fisher Scientific, Johannesburg, South Africa), hygromycin (Sigma-Aldrich), Trypsin-Versene® ethylenediaminetetraacetic acid (EDTA) (Lonza, Whitehead Scientific (Pty) Ltd, Cape Town,

* Corresponding author.
*E-mail address:* Minja.Gerber@nwu.ac.za (M. Gerber).

https://doi.org/10.1016/j.jddst.2023.104898
Received 8 June 2023; Accepted 29 August 2023
Available online 1 September 2023

South Africa) and Trypan Blue solution (0.4%) (HyClone, Separations, Johannesburg, South Africa) were utilised during the cytotoxicity studies.

## 3. Methods

### 3.1. Quantification of colchicine

An HPLC method for colchicine was developed and validated, in which all the chromatographic conditions were controlled. There was a Shimadzu® Nexera-I LC-2040C 3D HPLC, equipped with a quaternary pump, column heater, diode-array detection (DAD) detector and auto-sampler injector mechanism, connected to a LabSolutions Rev. A.10.03 acquisition and analysis software, which analysed the chromatograms. The laboratory in which the apparatus was stationed maintained a temperature of ±23 °C. A Venusil XBP $C_{18}$(2) reverse phase column (150 × 4.6 mm) (Agela Technologies, Newark, Germany) with a particle size of 5 μm was used. The mobile phases consisted of two Phases (A and B). Phase A consisted of UP water with 0.1% v/v analytical grade formic acid. Phase B consisted of acetonitrile with 0.1% v/v formic acid. Isocratic elution was used with 35% of mobile phase A and 65% of mobile phase B. A flow rate of 0.8 ml/min and UV detector (235 nm) were set accordingly for the detection of colchicine. Moreover, colchicine had a retention time of 4.2 min with a total run time of 5.0 min. The calculation of the limit of detection (LOD) and limit of quantification (LOQ) of colchicine was as 0.30 μg/ml and 0.93 μg/ml, respectively.

### 3.2. Preparation of a standard solution

A standard solution was prepared for each analysis. This standard solution and two dilutions were prepared and injected into the HPLC to acquire a linear regression curve. Each standard solution was prepared by adding 25 mg of colchicine into a 100 ml volumetric flask and filled to volume with chromatography grade methanol. There was 5 ml of the standard solution transferred to a 50 ml volumetric flask, and diluted to volume with chromatography methanol, resulting in Dilution 1; thereafter, 5 ml of Dilution 1 was filled to volume with chromatography grade methanol in a 50 ml volumetric flask, resulting in Dilution 2. Each sample was filtered using a 0.45 μm polyvinylidene difluoride (PVDF) filter and transferred to a marked HPLC vial for analysis. Once each HPLC vial was placed into the HPLC chamber, each sample was injected at different volumes of 2.5, 5.0, 7.5, 10.0, 20.0 and 25.0 μl, respectively. Following this there was a linear regression curve produced with an $R^2$ value of 1.00.

## 4. Physicochemical properties of colchicine

### 4.1. Solubility of colchicine in PBS (pH 7.4)

A water bath (Grant® JB series water bath, Grant Industries, Cambridgeshire, United Kingdom) equipped with a Variomag® magnetic stirring plate (Variomag, Daytona Beach, United States of America) was pre-heated at ~32 °C to maintain the epidermal surface temperature ([10] Pineau et al., 2012). Thereafter, four marked test tubes were filled with a volume of 5 ml PBS (pH 7.4) with one test tube used as the placebo (control – PBS (pH 7.4) containing no API), the remaining three were oversaturated with colchicine. There was a magnetic stirring rod placed into each test tube and inserted into the water bath; the samples were left to dissolve for 24 h. Each saturated sample was filtered using a 0.45 μm PVDF filter and 1 ml of each filtered sample was pipetted and transferred to a 100 ml volumetric flask and diluted to 100 ml with methanol (chromatography grade). Each diluted sample was sonicated for 5 min (using an Elma Transonic EL540 (Elma Schmidbauer GmbH, Singen (Hohentwiel) ultrasonic bath)), to ensure adequate dissolution. Each diluted solution (1 ml) was filtered using a 0.45 μm PVDF filter and transferred to marked HPLC vials for duplicate analysis. The placebo test tube followed the same method for the other three samples and analysed as the control solution [11].

### 4.2. Solubility of colchicine in n-octanol

To establish whether colchicine exhibits improved solubility in a lipophilic phase, the same method as mentioned for the solubility in PBS (pH 7.4) was followed, except *n*-octanol was used instead of PBS (pH 7.4). Furthermore, 1 ml of the colchicine saturated *n*-octanol solution was diluted in 50 ml methanol before injection into the HPLC to ensure safe use in the HPLC [11].

### 4.3. Solubility of colchicine in evening primrose oil

The solubility of colchicine in EPO was determined by a solubility test, following the same method as mentioned for the solubility in PBS (pH 7.4), except there was EPO used instead of PBS (pH 7.4); however, the 1 ml of the colchicine saturated EPO was filtered using 0.2 μm polytetrafluoroethylene (PTFE) filters, before undergoing dilution with methanol (chromatography grade). The HPLC analysis of each sample was in duplicate.

### 4.4. Octanol-buffer distribution coefficient of colchicine

There were equal volumes (10 ml) of *n*-octanol and PBS (pH 7.4) transferred into a beaker, containing a magnetic stirrer, and mixed on a hot plate for a period of 24 h, ensuring co-saturation of both phases. Thereafter, the co-saturated phases were transferred to a separating funnel to allow the separation of the phases. Once phase separation had occurred, both phases underwent separation into individually marked beakers (the top layer consisted of *n*-octanol and the bottom layer of PBS (pH 7.4)). Into three polytops (each containing a magnetic stirrer), there was 2 ml of pre-saturated PBS (pH 7.4) added. Thereafter, 324 mg of colchicine was added to each polytop sample and placed in a Grant® JB series water bath (Grant® JB series water bath, Grant Industries, Cambridgeshire, United Kingdom) (pre-heated ~32 °C) with a Variomag® magnetic stirring plate (Variomag, Daytona Beach, United States of America) to rotate for 45 min. *n*-Octanol (2 ml) was added to each polytop containing PBS (pH 7.4) with colchicine and left in a shaker water bath (pre-heated ~ 32 °C) to rotate for 2 h. Once removed from the water bath, the three *n*-octanol/PBS colchicine samples were transferred to three falcon tubes for centrifugation at 11 000 rpm for 30 min. The supernatant (*n*-octanol; 1 ml) from each sample was diluted to 100 ml, using chromatographic grade methanol, and filtered through a 0.45 μm PTFE filter into a marked HPLC vial for analysis in duplicate. PBS (from the bottom layer of the falcon tube; 1 ml) was extracted using a micropipette and diluted with chromatographic grade methanol to 100 ml. Each PBS (pH 7.4) dilution was filtered through a 0.45 μm PTFE filter into a marked HPLC vial for analysis in duplicate. The octanol-buffer distribution coefficient (log D) was determined using the concentration ratio of colchicine that was detected in *n*-octanol and PBS (pH 7.4), respectively. Using Equation (1), the log D value of colchicine was calculated [11].

$$\text{Log D} = \frac{\text{Concentration of colchicine in } n-\text{octanol}}{\text{Concentration of colchicine in PBS (pH 7.4)}} \qquad \text{Equation 1}$$

### 4.5. Formulation of hydrogel containing colchicine

There were three hydrogels formulated to contain 2% colchicine with different concentrations (w/w) of Carbopol® Ultrez 20 (gelling agent). Carbopol® Ultrez 20 and colchicine were dissolved in the aqueous phase (UP water; ~80 °C) on a magnetic hot plate. Once all components in the aqueous phase dissolved, and allowed to cool to room temperature (25 °C), each hydrogel was homogenised for 3 min. Each hydrogel was neutralised with a few drops of NaOH until there was an

appropriate pH reached and an adequate gel structure formed. The selected optimised hydrogel received the name **HG** (Table 1). Additionally, the formulation of a placebo **HG** (lacking colchicine), named **PHG**, was to function as a control group.

### 4.6. Formulation of emulgel containing colchicine

There were three emulgels containing colchicine (2%), surfactants and different concentrations of Carbopol® Ultrez 20 (w/w) formulated. Due to colchicine's good aqueous solubility (vs EPO solubility) and for comparison purposes to the **HG** (which contained colchicine within its aqueous phase), colchicine was incorporated into the aqueous phase containing Carbopol® Ultrez 20 and Tween® 80 (hydrophilic surfactant), which was then heated to ~80 °C on a magnetic hot plate. Separately, EPO (oil phase) was heated to ~80 °C on a magnetic hot plate into which Span® 60 (lipophilic surfactant) was added. Once dissolution occurred in both phases, the addition of the oil phase was in a dropwise fashion to the aqueous phase, forming a course oil-in-water (o/w) emulgel, followed by homogenisation and neutralisation (NaOH) forming suitable emulgels for skin application. Once characterisation was complete, the selected optimised emulgel received the named **EG** (Table 1). Additionally, there was a placebo of **EG** formulated, named **PHG,** to function as a control group.

### 4.7. Formulation of nano-emulsion containing colchicine

Of note, there was colchicine incorporated into the oil phase (EPO) of each nano-emulsion, for the purpose of its penetration enhancing properties as nano-droplets, to improve the possible transdermal delivery of colchicine. There were four o/w nano-emulsions formulated, each consisting of EPO, UP water, colchicine (2%) and different ratios of surfactants: Span® 60 and Tween® 80. The aqueous phase consisted of UP water and Tween® 80 heated to ~80 °C on a magnetic hot plate, while colchicine and Span® 60 dissolved in EPO (~80 °C) on a separate magnetic hot plate. Thereafter, the oil phase (EPO, colchicine, and Span® 6) was added dropwise into the aqueous phase forming a coarse o/w emulsion. Once cooled to room temperature (25 °C), each course o/w emulsion underwent sonication using an ultrasonicator to form a nano-emulsion. The nano-emulsion that demonstrated the most optimal properties was selected and named **NE** (Table 1). Additionally, a placebo **NE**, named **PNE** was also formulated to function as a control group.

### 4.8. Formulation of nano-emulgel containing colchicine

There were four nano-emulgels (o/w) formulated using the selected **NE** with different Carbopol® Ultrez 20 concentrations (w/w). After adding Carbopol® Ultrez 20 to the aqueous phase containing Tween® 80, it was heated to ~80 °C on a magnetic hot plate. Span® 60 and colchicine were dissolved in EPO (oil phase) at ~80 °C on a magnetic hot plate. Thereafter, the oil phase was added dropwise into the aqueous phase forming a coarse emulgel. There were nano-emulgels formed and each emulgel was homogenised and neutralised (NaOH) to ensure adequate gel formation. The selected optimised nano-emulgel was **NEG** (Table 1). Additionally, the formulation of a placebo **NEG**, named **PNEG,** was to function as a control group.

**Table 1**
Formula used to produce the different drug delivery vehicles.

| Phase | Excipients | Drug delivery vehicles (% w/w) | | | |
|---|---|---|---|---|---|
| | | HG | EG | NE | NEG |
| Oil | Colchicine | – | – | 2.0 | 2.0 |
| | EPO | – | 10.0 | 20.0 | 20.0 |
| | Span® 60 | – | 1.6 | 8.0 | 8.0 |
| Aqueous | Colchicine | 2.0 | 2.0 | – | – |
| | Carbopol® Ultrez 20 | 0.6 | 0.3 | – | 0.3 |
| | Tween® 80 | – | 0.4 | 2.0 | 2.0 |
| | UP water | 97.4 | 85.7 | 68.0 | 71.0 |

## 5. Characterisation of each drug delivery vehicle

### 5.1. Visual examination

After formulation of each drug delivery vehicle, a visual examination took place to ensure no visual instabilities were present, such as creaming, flocculation and sedimentation. Visual examination occurred on Days 1, 3 and 7.

### 5.2. pH

pH measurements, implemented in triplicate, were with a Mettler Toledo® pH meter (Mettler Toledo, Columbus, United States of America). Before pH measurements occurred, the pH meter was calibrated at pH values of 4, 7 and 10. Thereafter, the Mettler Toledo® InLab® 410 electrode was placed into each drug delivery vehicle to measure its pH values in triplicate [11].

### 5.3. Droplet size and polydispersity index

A Malvern Zetasizer Nano ZS (Malvern Instruments, Malvern, United Kingdom) measured the droplet size and polydispersity index (PDI) of each drug delivery vehicle in triplicate. One drop of each drug delivery vehicle (**HG**, **EG**, **NE** and **NEG**) was placed in separate 100 ml volumetric flasks and filled up to volume with UP water. Each volumetric flask was placed in an ultrasonic water bath to ensure adequate dissolution, and each sample (2 ml) transferred to disposable clear cuvettes followed by measurements in triplicate [11].

### 5.4. Zeta-potential

A Malvern Zetasizer Nano ZS (Malvern Instruments, Malvern, United Kingdom) measured the zeta-potential of each formulation in triplicate. The same method used for droplet size and PDI was used; however, clear disposable capillary zeta-cells were used containing 2 ml of each sample [11].

### 5.5. Viscosity

A Brookfield viscometer DV2T LV Ultra (Brookfield Engineering, Middleboro, United States of America) attached to a thermostatic water bath measured the viscosity. All drug delivery vehicles were placed in a preheated water bath at 25 °C for ±60 min before the viscosity was measured. Different spindles T-F (**HG**, **EG** and **NEG**), and T-B (**NE**) were attached to the viscometer and set to rotate at speeds (rpm) of 100 (**HG** and **EG**), 150 (**NE**) and 200 (**NEG**). The collection of the viscosity of each sample occurred at set multipoint time intervals of 2 min for 10 min [11].

### 5.6. Morphology

Transmission electron microscopy (TEM) images were taken using an FEI Tecnai G2 20S-Twin 200 kV high-resolution transmission electron microscope (HRTEM) (Czech Republic, Europe) fitted with an Oxford INCA X-Sight EDS System. TEM images were of the **NE** and its placebo (**PNE**) for the comparison of droplet sizes [11].

### 5.7. Entrapment efficiency

There were entrapment efficiency calculations performed on the nano-emulsions only. About 15 ml of each nano-emulsion sample was prepared and centrifuged at 23 000 rpm for 15 min at 23 °C. Thereafter, the oil and water phases were distinguishable. After extracting

supernatant of each sample (200 μl), it was diluted in a 5 ml volumetric flask with chromatography grade methanol. A small amount of each sample dilution was filtered using a 0.45 μm PTFE filter and placed in marked HPLC flasks for analysis. The samples were injected in duplicate. A standard solution and two dilutions thereof were prepared and injected into the HPLC as previously described, to obtain a linear regression curve for analysis of the samples [11].

The equation used for entrapment efficiency was as follows:

$$\text{Entrapment efficiency } (\%) = \frac{\text{Actual drug loading}}{\text{Theoretical drug loading}} \times 100 \qquad \text{Equation 2}$$

All **NEs** produced quite poor entrapment efficiency, with the selected **NE** producing the best entrapment efficiency of 32.376%.

### 5.8. Membrane release studies

Membrane release studies were performed with each drug delivery vehicle (**HG**, **EG**, **NE** and **NEG**) to determine whether colchicine was released from the different formulated drug delivery vehicles within the donor compartment of the Franz cells. There was PVDF membrane (Pall® Life Sciences, Port Washington, United States of America) placed between the donor and receptor phases of the Franz cell. Each Franz cell had Dow Corning® high vacuum grease moderately applied to both compartments (the top part of the receptor compartment and the bottom part of the donor compartment) to facilitate the two compartments' attachment. Before the attachment of both compartments, there was a small magnetic stirring rod placed inside each receptor compartment. Thereafter, PVDF membranes (Pall® Life Sciences, Port Washington, United States of America), consisting of a pore size of 45 μm and a diameter of 25 mm, were cautiously positioned on top of the receptor compartment. The vacuum-greased donor and receptor compartments were then attached (receptor compartment placed on top of donor compartment). Thereafter, there was vacuum grease applied to the sides/rims to seal the cells. Horseshoe clamps were fastened over the Franz cells, guaranteeing secure and intact cells, and preventing any leakage during the study. Preheated (~37 °C) PBS (pH 7.4; 2 ml) was injected into the receptor compartments of the Franz cells, while a visual inspection of the compartment ensured no air bubbles were present. Donor compartments were filled with the preheated (~32 °C) formulation (**HG**, **EG**, **NE** or **NEG**; two of the donor compartments were filled with the respective preheated (~32 °C) placebo vehicles (**PHG**, **PEG**, **PNE** or **PNEG**) to function as control groups. Parafilm® sealed the donor compartments. The prepared Franz cells were placed in a Franz cell stand and immersed into the preheated Grant® JB series water bath (~37 °C) (Grant® JB series water bath, Grant Industries, Cambridgeshire, United Kingdom) equipped with a Variomag® magnetic stirring plate (Variomag, Daytona Beach, United States of America). This guaranteed the magnetic stirring within each receptor compartment for the predetermined period in the water bath. After extracting the PBS from each receptor compartment, they were refilled with new PBS (pH 7.4, ~37 °C) at 1 h intervals for a period of 6 h. The receptor phase solution was transferred to marked HPLC vials for HPLC analysis to determine the concentration of colchicine released [11–13].

### 5.9. Skin diffusion studies

#### 5.9.1. Skin preparation

Only once ethical the North-West University Health Research Ethics Committee (NWU-HREC) had granted authorisation (Ethics no: NWU-00111-17-A1-13) could skin diffusion (*in vitro*) studies commence. After obtaining informed consent, skin collection was from female Caucasian donors undergoing abdominoplasty. Once collected, the skin samples underwent inspecteion for damage and abnormalities before preparation for the Franz cell studies. To achieve dermatomed skin samples with a width of 400 μm, a Zimmer® electric dermatome (Zimmer 201 TDS, United Kingdom) was pressed against the skin at an angle of 30–45°. After placing each skin sample on Whatman® filter paper and wrapping them in aluminium foil, they were stored in a freezer at −20 °C. Prior to the commencement of skin diffusion studies, the skin samples were removed from the freezer, thawed and cut into small circles to fit between the two compartments of each Franz cell [11,12,14,15].

#### 5.9.2. In vitro skin diffusion studies

A similar method as mentioned before (under membrane release studies) completed the skin diffusion studies on each drug delivery vehicle (**HG**, **EG**, **NE** and **NEG**). However, circular cut, dermatomed skin samples were positioned between the two Franz cell compartments (instead of a PVDF membrane), with the stratum corneum facing upward, in the direction of the donor compartment. After extracting the PBS from each receptor compartment, they were refilled with new PBS (pH 7.4, ~37 °C) at 2 h intervals for a period of 12 h. The receptor phase solutions were transferred to marked HPLC vials for HPLC analysis to determine the concentration of colchicine, which diffused through the dermatoned skin [11,12].

#### 5.9.3. Tape stripping

Once skin diffusion studies were completed, and each Franz cell's compartments detached, the skin sample underwent visual inspection, then removed and pinned to a small piece of Parafilm® on a solid surface. The skin sample was gently dabbed to remove excess drug delivery vehicle. Each pinned skin sample was tape stripped using ±16 pieces of 3 M Scotch® Magic™ tape, cut into small pieces to fit over the skin diffusion area. Rejection of the first strip of tape was to avoid contamination. The ±15 Scotch® Magic™ tape strips that remained, were pressed against the diffusion area and placed into a marked polytop filled with 5 ml methanol (extraction solution) [16]. The remaining tape-stripped skin samples were cut into smaller pieces, and placed in marked polytops filled with 5 ml methanol. All marked polytops were left overnight (±10 h) in a refrigerator at ~4 °C. Thereafter, a small volume of each solution from each marked polytop was filtered (0.45 μm PTFE filter) into marked HPLC vials for analysis [16,17]. The marked polytop samples (containing tape strips or pieces of skin) were analysed and compared to a regression curve to determine the concentration of colchicine present in the stratum corneum epidermis (SCE) and epidermis-dermis (ED), respectively [11,12,14,15].

#### 5.9.4. In vitro cytotoxicity assays

The epidermis consists mainly of keratinocytes, which compromise roughly 90–95% of the skin cells [18]. Therefore, there can be an investigation of cytotoxicity on human epidermal keratinocyte (HaCaT) cells, as established by Professor N. E. Fusenig [19,20]. Moreover, fibroblasts are a vital constituent for the construction of skin substitutes consisting of dermal and epidermal components [21]. Fibroblasts are conventionally associated with a structural component, involved in the synthesis of extracellular matrix [22]. BJ-5ta cells are human skin fibroblast cells immortalised with human telomerase reverse transcriptase (hTERT) [23,24]. Therefore, in this study the extent of cytotoxicity exposed to HaCaT and BJ-5ta cells were investigated through the exposure to **NE** (containing colchicine), **PNE** (absent of colchicine), and the **API** (colchicine). The high viscosity characteristic of the **HGs**, **EGs** and **NEGs** proved to be limiting, therefore it was not possible to perform cytotoxicity studies on these formulations.

#### 5.9.5. Cell culturing conditions

Both HaCaT and BJ-5ta cells were kept in a flask consisting of DMEM with high glucose, L-glutamine (4.0 mM) and sodium pyruvate, L-glutamine (2.0 mM), 1% NEAAs, 1% penicillin/streptomycin (10000 U/ml) (HaCaT cell line) and 10% FBS and hygromycin (5 mg/ml) (BJ-5ta cell line). The two cell lines cells were incubated in an ESCO Cell Culture $CO_2$ incubator (ESCO Technologies, Inc., Missouri, United States of America) at 37 °C in a 95% humidified atmosphere with 5% $CO_2$. Every second day there was an inspection of the cells and their growth media

replaced. Once the cells reached a confluency of ±80–90% trypsinisation (the removal of cells from their culture vessel for additional applications) [25,26] commenced to obtain a single cell suspension. Using the exclusion method, Trypsin-Versene® EDTA and Trypan Blue solution (0.4%) determined the concentration of viable cells present. The HaCaT and BJ-5ta cell suspension were diluted to obtain concentrations of 75 000 cells/ml and 60 000 cells/ml, respectively. By transferring 200 μl of the individual cell suspensions to the wells of the different assays the required density of cells was reached (per well 15 000 for the HaCaT and 12 000 for the BJ-5ta cell lines). To ensure appropriate cell recovery before treatment could commence, the seeded plates were incubated for a period of 24 h. After incubation, the cells were treated with different concentrations of colchicine (API), **NE** and **PNE** for 12 h.

#### 5.9.6. Methylthiazolyl tetrazolium (MTT) assay

There was identical treatment of both the HaCaT and BJ-5ta cell lines. Once the 12 h treatment exposure period had elapsed, the treatment solution aspirated from each well and rinsed twice with 100 μl of phosphate buffered saline. The dead cells were killed after 15 min once 200 μl of Triton™ X-100 (0.2% in phosphate buffered saline) had been added. The dimethyl sulfoxide (DMSO) blank wells were filled with 200 μl of preheated non-additive DMEM, while the untreated, treated, and dead wells were filled with 180 μl of preheated non-additive DMEM. Wrapped in aluminium foil, as the MTT-solution is light sensitive, each cell tray was placed in the $CO_2$ incubator for 4 h, at a temperature of 37 °C, 95% humidity and 5% $CO_2$. Thereafter, each well was aspirated and filled with 200 μl of DMSO to dissolve the formed crystals. To dissolve the formazan crystals, the plates were covered in aluminium foil, and placed on a shaker for 1 h. A SpectraMax™ Paradigm™ multimode microplate reader (Molecular Devices, California, United States of America) analysed each plate and the absorbance was set to measure at a cell signal of 560 nm with a background signal of 630 nm.

#### 5.9.7. Neutral red assay

The NR-assay also contained the same control groups as mentioned for the MTT assay, with the DMSO replaced with a solubilisation blank as the only difference. Once the treatment period had elapsed, all wells were aspirated and rinsed twice with 100 μl of phosphate buffered saline. Thereafter, non-additive DMEM (200 μl) and 200 μl of the filtered 10.00% (v/v) NRS was added up to volume to the untreated, treated, and dead cell control wells. Both plates were covered with aluminium foil and incubated for 2 h. Once the 2 h incubation period had elapsed, each well was aspirated and 100 μl of NR-fixative (1% calcium chloride ($CaCl_2$)) in 0.5% formaldehyde) added to the wells for fixation. Finally, 150 μl of NR-solubilisation solution (1% acetic acid in 50% ethanol) was added to the wells. The plates were then covered and placed on a shaker for 10 min. The same plate reader as mentioned for the MTT assay read the plates, while the absorbance was set to measure at a cell signal of 540 nm with a background signal of 690 nm.

#### 5.9.8. Statistical data analysis

STATISTICA® 13.3 (StatSoft, TIBCO® Software Inc., Palo Alto, United States of America) statistically analysed the obtained data. For each drug delivery vehicle during the different diffusion (membrane release and *in vitro* diffusion) studies and tape stripping experiments, there were descriptive statistics completed, using box-plots, average and median values.

## 6. Results and discussion

### 6.1. Physicochemical properties of colchicine

#### 6.1.1. Solubility of colchicine in PBS (pH 7.4), n-octanol and evening primrose oil

The calculation of the experimental solubility of colchicine in PBS (pH 7.4) was 14.339 ± 0.993 mg/ml. Colchicine's exhibits an acceptable solubility value for transdermal diffusion, as the aqueous solubility was above 1 mg/ml, which is ideal for transdermal drug delivery [27,28].

The calculation of the solubility of colchicine in *n*-octanol and EPO was 162.090 ± 25.585 and 0.209 ± 0.045 mg/ml, respectively. These results demonstrated that colchicine is relatively poorly soluble in EPO compared to its lipid solubility in *n*-octanol. This can be a result of the complexity of API solubilisation in lipids (EPO) [29]. Many kinetic and thermodynamic factors, including physical and chemical environment, interfacial tension, molecular volume, etc., influence the solubilisation of APIs in lipids [29].

#### 6.1.2. Octanol-buffer distribution coefficient of colchicine

The calculation of log D of colchicine was 1.196. The octanol-water partition coefficient (log P) and the log D are both relevant to drug delivery, as they describe lipophilicity [30]. This log D value calculated for colchicine is close to the log P value stated by Ref. [31] for colchicine as 1.300 [32]. In addition, molecules with a log P value in the 1.000–3.000 range exhibit both aqueous and lipophilic properties [32]. Therefore, the conclusion is that colchicine possesses both hydrophilic and lipophilic properties. Furthermore, APIs with a log P value of between 1.000 and 3.000, such as colchicine, are optimal for the possible transdermal drug delivery [28].

### 6.2. Characterisation of each drug delivery vehicle

#### 6.2.1. Visual examination

All drug delivery vehicles (displayed in Fig. 1) showed no signs of physical instabilities, such as creaming, sedimentation and/or flocculation. All formulated gels (**HG**, **EG** and **NEG**) were glossy and smooth in appearance, while all **NEs** were milky in appearance and consistency.

#### 6.2.2. pH

All drug delivery vehicles (**HG**, **EG**, **NE** and **NEG** in Table 2) measured a pH within the range of 5–9, where no skin irritation was expected to occur and therefore, all vehicles were deemed safe for skin application [28].

#### 6.2.3. Droplet size and PDI

Droplet size (displayed in Table 2) is a vital consideration when assessing skin permeation [33]. The **NE** measured an ideal droplet size of smaller than 100 nm and could be a nano-emulsion. The **NEG** consisted of the **NE** and a gelling agent (Carbopol® Ultrez 20). Carbopol® Ultrez 20 is characterised by a large molecular weight (100 Megadalton (MDa)), which may have affected the average droplet size within the **NEG**, resulting in its droplet size measuring larger than 100 nm [34]. The **HG** measured a droplet size >100.0 nm and <0.1 mm and could therefore be classified as a microgel [35–37]. Moreover, the **EG** measured a droplet size larger than 400 nm, therefore, characterising it as a macroemulsion with a gelling agent [38].

The PDI of a formulation is an important physical property and described as the "degree of homogeneity of particles" [39]. A very low PDI value (that closest to zero) is indicative of a homogenous formulation containing a narrow droplet size distribution. Comparatively, a PDI measurement of closer to one (1.0) may indicate a large distribution of droplet sizes [40,41]. The **NE** measured the best PDI (closest to 0), characterising it as the most homogenous drug delivery vehicle with a narrow size distribution. The **NE** was followed by the **EG**, **NEG** and finally, the **HG** exhibited the poorest PDI, indicating that it was more heterogeneous with the largest size distribution.

#### 6.2.4. Zeta-potential

The stability of a dispersion is function dependent on zeta-potential and it is a measure of the overall charges [42]. A satisfactory measure of zeta-potential is +30 mV or −30 mV, which allows adequate electrostatic repulsion, inhibiting aggregation within the drug delivery vehicle

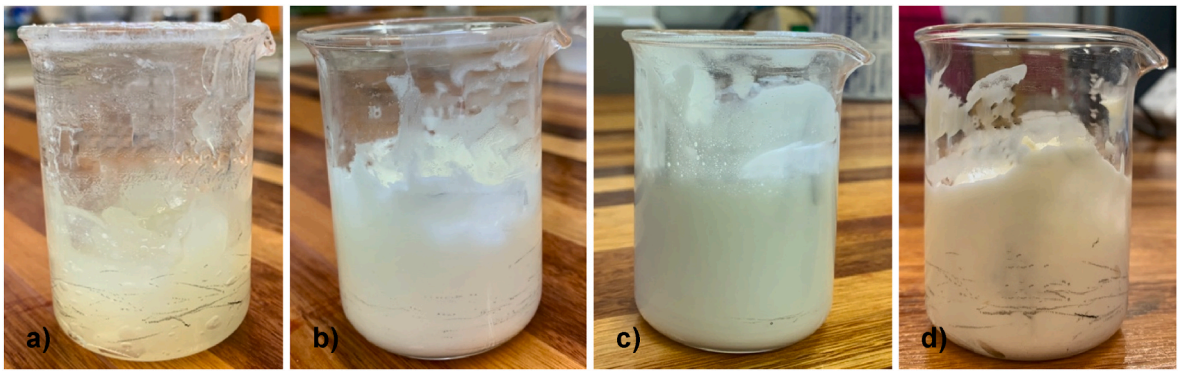


**Fig. 1.** Visual examination of the optimised drug delivery vehicles a) **HG**, b) **EG**, c) **NE** and d) **NEG**.

**Table 2**
A summary of each drug delivery vehicle's characterisation.

| | HG | EG | NE | NEG |
|---|---|---|---|---|
| pH | 6.160 ± 0.020 | 6.136 ± 0.015 | 6.300 ± 0.004 | 6.177 ± 0.005 |
| **Droplet size (nm)** | 221.50 ± 22.60 | 1331.00 ± 150.90 | 96.48 ± 1.15 | 211.00 ± 3.57 |
| **PDI** | 0.518 ± 0.049 | 0.342 ± 0.150 | 0.178 ± 0.002 | 0.435 ± 0.111 |
| **Zeta-potential (mV)** | −88.8 ± 2.0 | −67.2 ± 0.7 | −34.9 ± 7.0 | −58.3 ± 0.2 |
| **Viscosity (cP)** | 6525.6 ± 297.6 | 6367.4 ± 188.4 | 64.0 ± 1.0 | 3233.4 ± 15.6 |

[39,42]. All formulated drug delivery vehicles measured adequate zeta-potential measurements, deeming them all physically stable (illustrated in Table 2). The lowest zeta-potential measurement was recorded for the **HG**, followed by the **EG**, **NEG** and finally, the **NE** measured the largest zeta-potential. Carbopol® Ultrez 20 can improve a vehicle's zeta-potential, which is evident in Table 2, where all vehicles containing Carbopol® Ultrez 20, demonstrated improved zeta-potential measurements compared to the **NE**, which lacked a gelling agent.

### 6.2.5. *Viscosity*

The viscosity of a transdermal delivery vehicle can influence its API delivery across the skin, directly influencing its API diffusion rate [43]. Each drug delivery vehicle measured different viscosity measurements (displayed in Table 2), due to their different components. All the vehicles that contained Carbopol® Ultrez 20 (the **HGs**, **EGs** and **NEGs**) measured higher viscosity measurements in comparison to the **NEs**. There was an increase in viscosity and elasticity noted once there was NaOH added to the vehicles containing Carbopol® Ultrez 20, since Carbopol® Ultrez 20's reaches its maximum viscosity at a pH measurement of 6–7 [34,44]. The high viscosity measurement of each **HG**, **EG** and **NEG** may result in slower, more retarded API delivery through the skin [45], while the low viscosity of **NEs** circumvents coalescence between droplets and ensures their appeal in the industry [46,47].

### 6.2.6. *Morphology*

TEM images of both **NE** and **PNE** exhibited the droplet size of both samples. Fig. 2 demonstrates that the droplets within the **NE** (Fig. 2a) were spherical in shape and did not suggest any coalescence, signifying the possible stability of the **NE** [48]. The TEM image of the **NE** validates the droplet size measurements (Table 2), as most droplets within **NE** measured within the nano-range (<100 nm). The **PNE** had larger droplet sizes than the **NE**, which may be due to the droplets being extremely close together, as seen in Fig. 2b and 2c. This may cause the destabilisation of the nano-emulsion in the future due to Ostwald ripening [49].

### 6.2.7. *Entrapment efficiency*

The entrapment efficiency was poor for all four **NEs** (**NE1** to **NE4**), which might be attributed to colchicine's hydrophilic nature, causing colchicine to move into the aqueous phase of each **NE**, resulting in less API within the oil phase, producing poor drug entrapment efficiency (%) [50]. However, **NE4** (the final selected **NE**) exhibited the highest API entrapment efficiency (32.376%), followed by **NE3** (31.281%), **NE2** (31.264%) and lastly, **NE1** measured the poorest API entrapment at 30.721%.

## 6.3. *Diffusion experiments*

### 6.3.1. *Membrane release studies*

The membrane release studies used the median values of all the collected data (displayed in Table 3) for the discussion of the membrane release studies, as the median values were more accurate and less

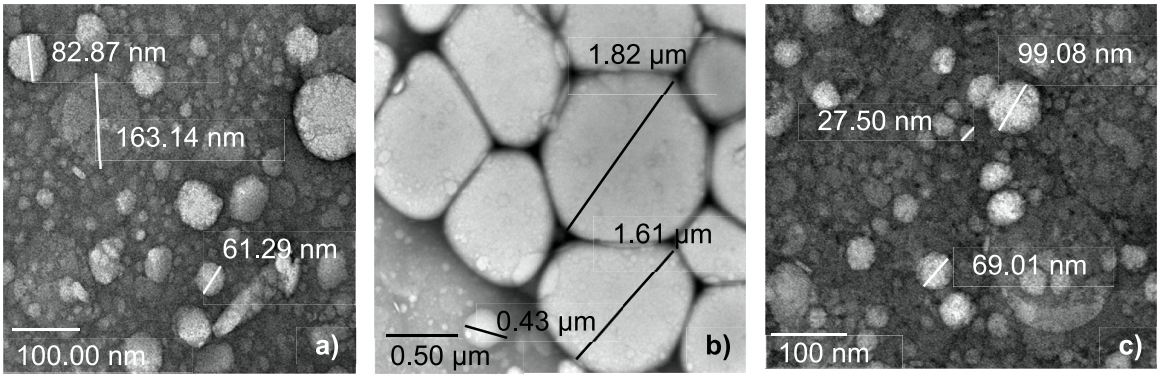


**Fig. 2.** TEM micrographs of **NE** (a) and **PNE** (b and c).

**Table 3**
Average and median flux values obtained from membrane release studies ($n$ = number of skin samples).

| Drug delivery vehicle | $n$ | Average % release (%) | Average flux (μg/cm$^2$.h) | Median flux (μg/cm$^2$.h) |
|---|---|---|---|---|
| **HG** | 10 | 0.754 ± 0.133 | 41.976 ± 7.340 | 40.3278 |
| **EG** | 11 | 0.868 ± 0.158 | 420.071 ± 46.730 | 406.1751 |
| **NE** | 11 | 2.959 ± 0.249 | 102.759 ± 10.840 | 101.7896 |
| **NEG** | 11 | 3.093 ± 0.519 | 123.080 ± 16.050 | 124.6087 |

affected by outliers [51]. Furthermore, Fig. 3 was included to display the membrane release results obtained. It is important to note that membrane release studies establish whether an API is released from its formulations, into which it is incorporated to ensure that skin diffusion studies can be conducted [14]. Through the comparison of the median flux (μg/cm$^2$.h) values of each drug delivery vehicle, the conclusion was that the **EG** exhibited the highest flux through the membrane, followed by the **NEG**, **NE** and finally, the **HG**, which measured the lowest flux.

The **HG's** poor flux may be due to the PVDF membrane, which is a hydrophobic membrane that imposes the penetration of hydrophilic vehicles (such as the **HG**) [52]. Colchicine was dissolved in the aqueous phase of the **HG** (hydrophilic), which lacked an oil phase; therefore, the PVDF membrane may have limited the release of colchicine from this vehicle (which was extremely hydrophilic in comparison to the other three vehicles) to the receptor compartment, resulting in a lower flux.

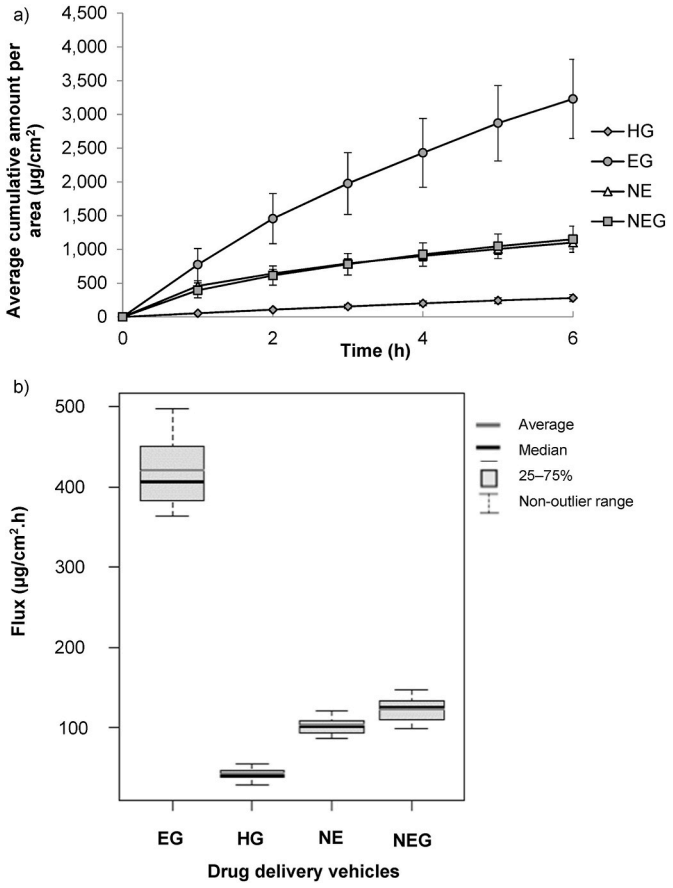


**Fig. 3.** a) Average cumulative amount of colchicine released per area (μg/cm$^2$) over 6 h during the membrane release studies from all the drug delivery vehicles, and b) box-plot displaying the average and median flux (μg/cm$^2$.h) of colchicine for the drug delivery vehicles during the membrane release studies over a period of 6 h.

Between the flux of the **NEG** and **NE**, it is evident that the **NEG** demonstrated an improved median flux, which could be a result of its gelling agent, as this was the only difference between the two formulations. The incorporation of a **NE** into an emulgel system (producing a **NEG**) can influence the release of the API from its gel matrix. Ordinarily, a gel component within a formulation forms a film, which likely retards the flux of an API; however, there was no such experience in this study [53].

The **EG's** superlative flux may be the result of colchicine's improved aqueous solubility, as colchicine exhibited a better aqueous solubility (in UP water) compared to that of EPO. Colchicine was also included in the water phase of the **EG** for comparison purposes to the **HG**. Hence, colchicines improved solubility in the aqueous phase of the **EG** may have significantly contributed in the **EG's** high flux, as only the dissolved portion of an API in a drug delivery vehicle can cross the membrane [55].

A one-way ANOVA indicated a statistically significant difference in the flux values between the groups ($p < 0.001$). Consequently, the Bonferroni post-hoc test investigated the differences between each of the drug delivery vehicles and showed statistically significant differences for all the pairwise comparisons ($p < 0.05$), except between the **NE** and **NEG**, which measured a p-value of 0.438 ($p > 0.05$). It is unlikely, that the statistically significant data generated between all the pairwise comparisons, occurred randomly but can rather be attributable to a specific cause [56]. These specific causes may be due to the different drug delivery vehicles and their different formulation characteristics.

Since all four vehicles successfully released colchicine from the formulation, there could be skin diffusion conducted.

### 6.3.2. *In vitro skin diffusion studies*

For accuracy purposes, the median values of all the collected data (displayed in Table 4) were used for the discussion of the *in vitro* skin diffusion studies [51]. Fig. 4 represents the skin diffusion data obtained during this study.

The average and median flux (μg/cm$^2$) of the **HG** and **EG** was determined over 6–12 h, oppositely, the average and median flux (μg/cm$^2$) for the **NE** and **NEG** was displayed at 4–10 h. According to their median flux (μg/cm$^2$.h) values, the ranking for the diffusion of colchicine from the drug delivery vehicles can be in increasing order: **EG** < **NEG** < **HG** < **NE**.

The **NE** measured the superlative median flux compared to the other vehicles (**HG**, **EG** and **NEG**). The **NEs** improved flux may be due to the small droplet size of the **NEs** in comparison to the other vehicles. Through the facilitated API transport of nano-sized droplets, an improvement in the rate of permeation of colchicine through the skin's barrier could be established [57]. Additionally, a **NEs** small droplet size can provide a substantial area for API permeation through the skin; subsequently, improving the concentration gradient of colchicine, resulting in its efficient transdermal drug delivery [58]. Moreover, due to a **NEs** possible hydration of the skin, improved penetration of colchicine may have occurred [59]. Additionally, one could attribute the decreased flux of the **HG**, **EG** and **NEG** (compared to the **NE**) to their gelling agent component. Through the addition of gelling agents (Carbopol® Ultrez 20) to transdermal vehicles, there is a film-forming effect created on the skin [53], which functions as an external reservoir,

**Table 4**
Average and median flux values obtained from *in vitro* skin diffusion studies ($n$ = number of skin samples).

| Drug delivery vehicle | $n$ | Average % release (%) | Average flux (μg/cm$^2$.h) | Median flux (μg/cm$^2$.h) |
|---|---|---|---|---|
| **HG** | 9 | 0.072 ± 0.020 | 1.8364 ± 0.500 | 2.1350 |
| **EG** | 9 | 0.057 ± 0.010 | 1.5426 ± 0.300 | 1.5721 |
| **NE** | 9 | 0.086 ± 0.028 | 2.8497 ± 0.010 | 2.8497 |
| **NEG** | 8 | 0.058 ± 0.010 | 1.8293 ± 0.320 | 1.9123 |

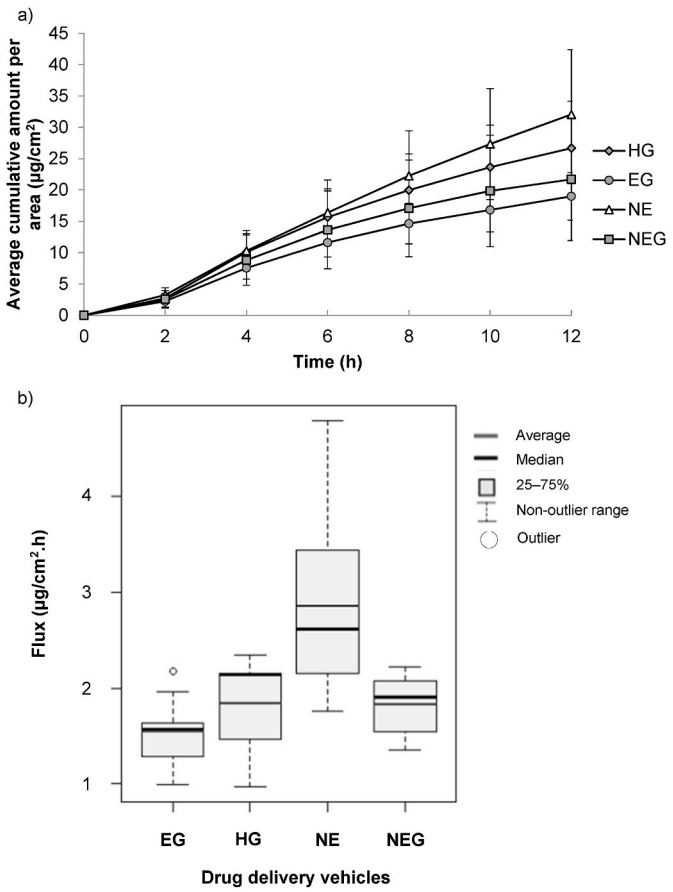


**Fig. 4.** a) Average cumulative amount of colchicine diffused per area (µg/cm$^2$) over 12 h during the *in vitro* skin diffusion studies from all the drug delivery vehicles, and b) box-plot displaying the average and median flux (µg/cm$^2$.h) of colchicine for the drug delivery vehicles during the skin diffusion studies (*in vitro*) over a period of 12 h.

causing a slow release of the API from the formulation into and through the skin [53]; subsequently, leading to a lower rate of diffusion (flux) of colchicine.

The hydrophilic **HG** (lacking an oil phase) demonstrated the second highest flux and the superlative flux between the gel-containing vehicles (**HG**, **EG** and **NEG**). This was unexpected, as the stratum corneum is lipophilic in character and is predominantly a barrier against hydrophilic entities such as the **HG** [60]. The transappendageal route (through skin appendages i.e., hair follicles and sweat glands) plays an important role in the transdermal pathways for hydrophilic APIs (i.e., **HGs**), ions, polar molecules and high molecular weight compounds but due to its limited availability on the skin (0.1–1.0% of the total skin surface area), it was believed that a different pathway may also have been followed by the **HG** [61–63]. Water is the safest and most simple penetration enhancer and during this study, the skin was in contact with the hydrophilic **HG** for a period of 12 h; thus, hydration of the skin occurred [64]. Through skin hydration, the lipophilic components of the skin become disrupted, improving the penetration of APIs and therefore, resulting in the **HGs** improved colchicine penetration through the skin [64,65]. In addition, colchicine (within the **HG**) was immediately available for diffusion into the skin compared to the **EG** and **NEG** (containing an oil phase), as colchicine within the **HG** did not need to partition through an oil phase (like the **EG** and **NEG**) before skin penetration could occur; therefore, resulting in the **HGs** improved skin penetration [63].

The median flux of **NEG** compared to that of the **EG** demonstrated improved skin penetration when compared to the **EG** counterpart. A possible reason for the enhanced permeation of the **NEG**, could be as a result of the droplet size [66], as the nano-droplets within the **NEG** tolerates a larger surface area for colchicine on the skin than the **EG**, resulting in a larger concentration gradient and finally, an improved delivery of colchicine across the skin [66].

Each drug delivery vehicle (average concentration diffused of **HG** (14.348 ± 4.027 µg/ml), **EG** (10.215 ± 2.051 µg/ml), **NE** (17.242 ± 5.553 µg/ml) and **NEG** (11.666 ± 2.028 µg/ml) was able to successfully surpass the suggested oral blood therapeutic dosing of colchicine, as described by Winek et al. as 0.0003–0.0300 µg/ml [67]. However, an important aspect to note of *in vitro* studies, is that the data cannot always correlate with the clinical situation (since skin activities like metabolism, enzymatic degradation, elimination, etc. are generally absent during *in vitro* skin diffusion studies) but should be a qualitative prediction [68].

A one-way ANOVA demonstrated a statistically significant difference in the flux values between the groups ($p < 0.001$); therefore, the Bonferroni post-hoc test was implemented to investigate the differences between each of the drug delivery vehicles. Statistical significances observed between the **NE** and both **EG** and **HG** was $p < 0.05$.

### 6.3.3. *Tape stripping*

The median concentration for both SCE and ED (Table 5) was used, since outliers affect the average concentration [51]. Fig. 5 displays a box-plot with the tape stripping data.

When comparing the median concentration of colchicine in the SCE and ED for each drug delivery vehicle, it was determined that **HG** measured the largest concentration in the SCE and ED followed by **EG**, **NEG** and finally, **NE**, which measured the lowest concentration in both the SCE and ED.

Regardless of the SCE's lipophilic nature [60], the **HG** exhibited the largest median concentration within the SCE, which might be attributed to the **HG's** hydration properties [65,69]. Through the hydration of the SCE, its lipid lamellar structure is disrupted, decreasing its barrier properties [59,70]. The result is visible in the swelling of the corneocytes within the skin's intercellular spaces (cisternae), as water accumulates [70]. Furthermore, the skin was hydrated for 12 h during the *in vitro* skin diffusion study before tape stripping took place, which may further have facilitated and improved the diffusion of colchicine from the hydrophilic **HG** into the hydrated SCE (and therefore, more hydrophilic) [59,71]. Both the ED and **HG** are described as hydrophilic [11], which may explain the **HGs** largest concentration of colchicine delivered to the ED, as colchicine may have partitioned out of the **HG** (which does not have an oil phase) into the favourable hydrophilic ED [72].

All EPO containing vehicles (**EG**, **NE** and **NEG**) measured less colchicine within the SCE and ED than the **HG**. Although EPO was incorporated as an oil phase to act as a penetration enhancer to bypass the limitations of the SCE [73], the fact that the SCE was hydrated for 12 h before tape stripping commenced may have resulted in a more hydrophilic SCE. This may have resulted in the possible delay of the permeation of colchicine from the o/w type vehicles (which are more lipophilic in nature in comparison to the hydrophilic **HG**) into the hydrated SCE (more hydrophilic due to accumulation of water) [70].

When comparing the results of the **NE** to those of the **NEG**, the **NE** measured a lower concentration of colchicine in both the SCE and ED, despite the only difference between the two vehicles being the inclusion of a gelling agent in the **NEG**. Although, colchicine was included in the oil phase of the **NEG** and **NE**, EPO still acted as a penetration enhancer, which allowed colchicine to penetrate the upper skin layer (SCE) and move into the ED [14]. The conclusion is that skin penetration enhancers can either decrease the barrier properties of the skin or actively force the movement of APIs across the skin [68]. Additionally, it was also observed that when comparing the **NE** to the gel-containing vehicles (**HG**, **EG** and **NEG**), the **NE** still measured the lowest median concentration in the SCE. This could most likely be due to the lack of gelling agent within the **NE**, as an addition of a thickening agent (such as in the

**Table 5**
Tape stripping data of the different drug delivery vehicle ($n$ = number of skin samples).

| Drug delivery vehicle | $n$ | Average concentration in SCE (μg/ml) | Median concentration in SCE (μg/ml) | Average concentration in ED (μg/ml) | Median concentration in ED (μg/ml) |
|---|---|---|---|---|---|
| **HG** | 9 | 1.856 ± 1.205 | 1.362 | 1.576 ± 1.222 | 1.232 |
| **EG** | 9 | 1.327 ± 0.383 | 1.296 | 1.052 ± 0.468 | 0.864 |
| **NE** | 9 | 0.457 ± 0.096 | 0.420 | 0.426 ± 0.410 | 0.364 |
| **NEG** | 8 | 0.545 ± 0.261 | 0.563 | 0.651 ± 0.320 | 0.475 |

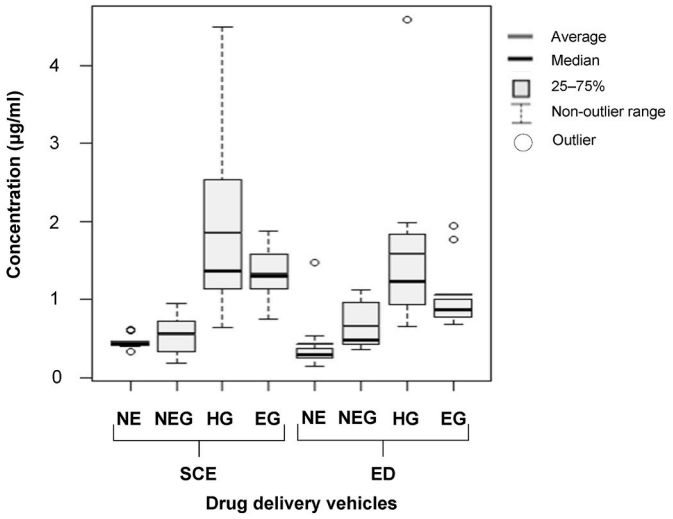


**Fig. 5.** Box-plot displaying the average and median concentration (μg/ml) of colchicine from the different drug delivery vehicles that was delivered in the SCE and ED after each 12 h skin diffusion study.

**HG**, **EG** and **NEG**) can increase a vehicle's affinity towards the SCE [11].

The nano-sized drug delivery vehicles (**NE** and **NEG**) measured higher API concentrations within the both the SCE and ED, when compared to the semi-solid vehicles (**HG** and **EG**). It was expected that the smaller droplet sized vehicles, i.e., the **NE** and **NEG**, would have produced higher API concentrations within the SCE [74–77] than those with larger droplet sizes (**HG** and **EG**), but it was revealed the semi-solid vehicles (**HG** and **EG**) had higher concentrations of colchicine in the SCE than the nano-sized vehicles (**NE** and **NEG**).

Finally, when comparing the **EG** to the **NEG**, both of which compromised emulgels, the **EG** measured a larger concentration of colchicine within the SCE and ED, than that of the **NEG**. The **EGs** superlative colchicine concentration in both skin layers may be due to the colchicine being incorporated in the water phase of the **EG**, while the colchicine was incorporated in the oil phase of the **NEG**. Therefore, the colchicine in the water phase of the **EG** will be readily available for skin penetration into the hydrated SCE, while the colchicine within the **NEG** will first have to partition out of the oil phase (EPO) before being available for skin penetration, delaying the permeation of colchicine into the SCE [63].

A two-way ANOVA was required to determine statistically significant differences; however, there was only a statistical significance between the formulation types ($p < 0.05$) and not the tape stripping methods (SCE and ED) ($p > 0.05$), which indicates that each drug delivery vehicle affected the tape stripping data. Thereafter a Bonferroni post-hoc test determined the comparison of the mean concentration of colchicine from each drug delivery vehicle and not the tape stripping methods (SCE and ED). There were statistically significant differences measured between the **HG** and **NE**, as well as the **HG** and **NEG** ($p < 0.05$), which concluded that the drug delivery vehicles affected the data and were not a cause of random circumstance [56].

### 6.3.4. *In vitro cytotoxicity assays*

The calculation of the viability of the cell cultures was relative to the untreated cell control, indicated as 100% viability [78]. The %viable cells were subtracted from the initial concentration of viable cells (100%), forming a regression line. Fig. 6 (HaCaT cell line) and Fig. 7 (BJ-5ta cell line) present the results expressed as graphs.

### 6.3.5. *Methylthiazolyl tetrazolium (MTT) assay*

Most of the HaCaT cells treated with **NE** exhibited no cytotoxicity (>80% cell viability). However, the HaCaT cells treated with 7.5 μg/ml **NE**, exhibited weak cytotoxicity (%cell viability of 60–80%) [79]. The **PNE** treated HaCaT cells showed no toxicity, as %cell viability across all concentrations was above 80% [79]. The HaCaT cells treated with the **API** exhibited weak cytotoxicity (%cell viability between 60 and 80%) at concentrations of 7.5, 12.5 and 15.0 μg/ml. However, the HaCaT cells treated with other concentrations of the **API** showed no cytotoxicity (80% cell viability) [79]. The BJ-5ta cells treated with the **NE**, **PNE** and **API** showed no cytotoxicity as all concentrations of **NE**, **PNE** and **API** exposed to the BJ-5ta cells resulted in a %cell viability >80% [79].

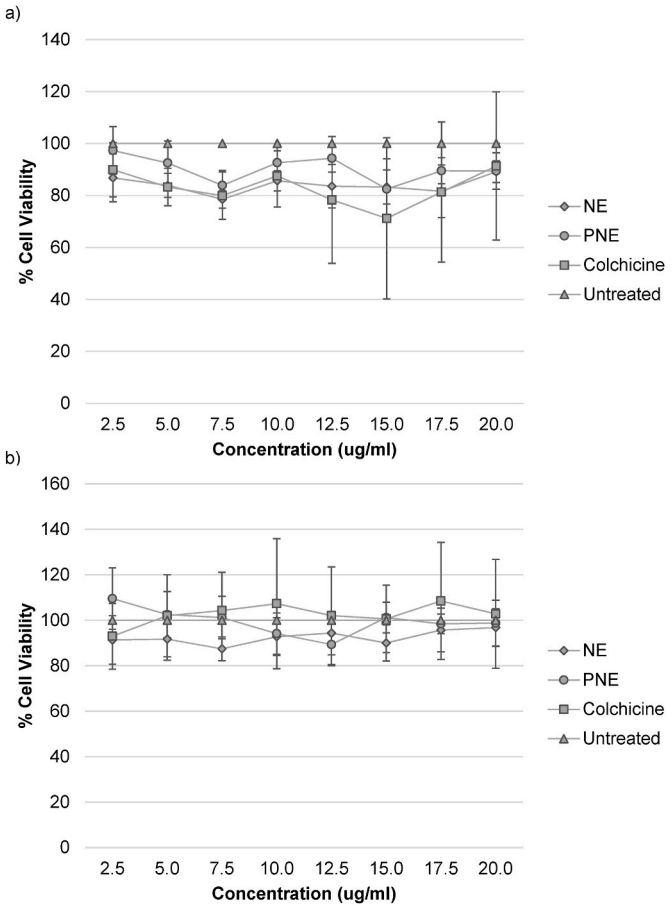


**Fig. 6.** %Cell viability of the HaCaT cells after a 12 h exposure to the different concentrations (μg/ml) of the **NE**, **PNE** and API treatments during the a) MTT- and b) NR-assays.

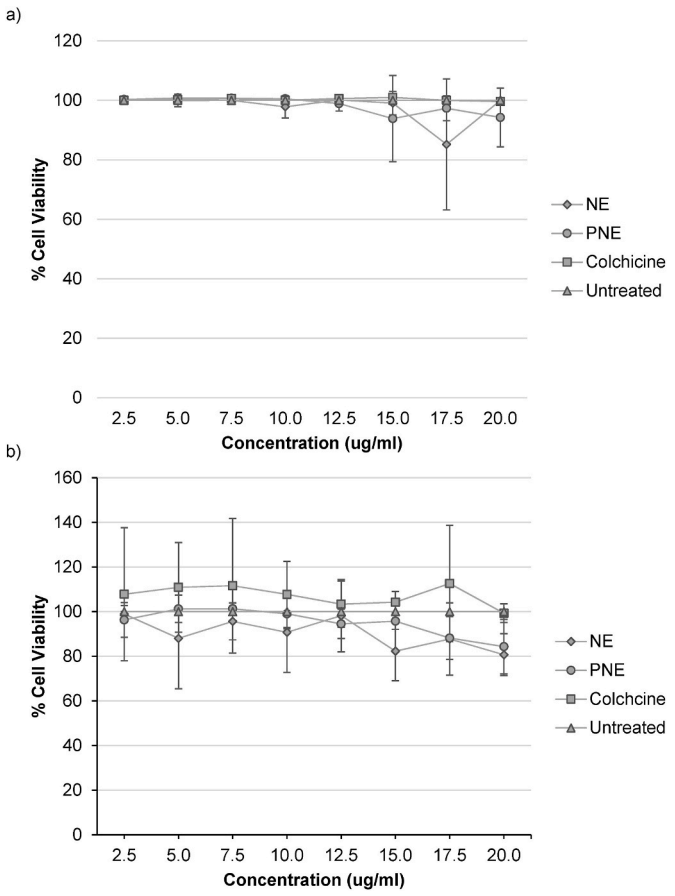


**Fig. 7.** %Cell viability of the BJ-5ta cells after a 12 h exposure to the different concentrations (μg/ml) of the **NE**, **PNE** and API treatments during the a) MTT- and b) NR-assays.

### 6.3.6. *Neutral red assay*

HaCaT and BJ-5ta cells treated with **NE**, **PNE** and **API** showed no toxicity, as %cell viability across all concentrations (2.5–20.0 μg/ml) was >80% [79].

## 7. Conclusion

Colchicine showed good lipophilic and hydrophilic properties according to its log D value; therefore, deeming it an ideal API for incorporation into four diverse transdermal drug delivery vehicles [28]. Colchicine was released from each drug delivery vehicle (**HG**, **EG**, **NE** and **NEG**) during the membrane release studies, which allowed colchicine to be successfully delivered through the skin (*in vitro* skin diffusion studies) and penetrate the skin's (SCE and ED). The **NE** was the most successful drug delivery vehicle to penetrate the skin (superlative skin flux and poor colchicine concentration within the SCE and ED), concluding that due to its nano-droplet size, it was able to penetrate deeper levels of the skin and deliver colchicine successfully to the systemic circulation [57,80]. The **HG** demonstrated the second highest flux during the *in vitro* skin diffusion studies. Due to the **HG's** large aqueous phase, hydration of the SCE could occur improving the flux of colchicine [36,70,71]. However, due to the hydration of the SCE (resulting in water accumulation within the cisternae) and hydrophilic nature of the ED, the **HG** measured the largest concentration of colchicine within both skin layers (SCE and ED), as it was able to diffuse into its preferred environment [36,70–72]. The **NEG** produced average results with regard to both its transdermal and topical delivery of colchicine, as it measured the third highest median flux through the skin and the second lowest concentration of colchicine within both the SCE and ED. The gelling agent within the **NEG**, formed a film-like layer on the skin, which may have retarded the release of colchicine from the **NEG**, as the film-forming layer on the skin possibly caused a reservoir effect, slowly releasing colchicine into the SCE, ED and finally, through the skin into the systemic circulation [53,54].

This study concluded that the solubility of an API within transdermal drug delivery vehicles and well as the drug delivery formulation plays an integral role in the ability of colchicine to be delivered into and through the skin [64,81].

Lastly, the cytotoxicity studies of the **API**, **PNE** and **NE** (at selected concentrations that diffused into and through the skin) concluded weak to no cytotoxic effects, as the MTT-assay determined that the **PNE** showed no cytotoxicity, while the **NE** and **API** exhibited weak to no cytotoxicity [79]. Furthermore, the three treatment groups (**NE**, **PNE** and **API**) showed no cytotoxicity on both HaCaT and BJ-5ta cell lines through the NR-assay.

## Credit author statement

Micaela Ponte (student) was the primary researcher responsible for performing the research, analysing the data, as well as drafting of the original research manuscript of this study. Minja Gerber conceptualised the study. Minja Gerber and Wilna Liebenberg supervised the project, attained funding, designed the study and assisted in writing the manuscript through critical reviewing and editing. All authors approved the submission to the journal and contributed to the final manuscript.

## Declaration of competing interest

None declared.

## Data availability

Data will be made available on request.

## Acknowledgements

The authors would like to give special thanks to the Centre of Excellence for Pharmaceutical Sciences (Pharmacen™) of the North-West University (NWU), Potchefstroom Campus, South Africa, for the financial support during these studies. The authors would also like to thank Prof. F. van der Kooy, from the Analytical Technology Laboratory (ATL), Pharmacen™, NWU, for his guidance during HPLC method development and validation, Dr. A. Jordaan (Laboratory for Electron Microscopy (LEM), Chemical Resource Beneficiation, NWU) for her expertise during the TEM characterisation of samples, Dr. O. Kunhle, from the Mammalian Cell Culture Laboratory in the Laboratory for Analytical and Molecular Biology (LAMB), Pharmacen™, NWU, for preparation and assistance during *in vitro* cytotoxicity studies and Dr. M. Cockeran, from the School of Mathematical and Statistical Sciences, NWU, who performed and analysed the statistical data required for the diffusion studies.

## References

[1] M.D. Harris, L.B. Siegel, J.A. Alloway, Gout and hyperuricemia, Am. Fam. Physician 59 (4) (1999) 925–934.
[2] Healio Rheumatology, Global cases of gout exceed 41 million with 'alarming rate' of increased burden. https://www.healio.com/news/rheumatology/20200901/global-cases-of-gout-exceed-41-million-with-alarming-rate-of-increased-burden, 2020. Date of access: 19 May. 2021.
[3] John Hopkins Arthritis Center, Gout. https://www.hopkinsarthritis.org/arthritis-info/gout/, 2021. Date of access: 19 May. 2021.
[4] E. Roddy, M. Doherty, Gout. Epidemiology of gout, Arthritis Res. Ther. 12 (6) (2010) 223, https://doi.org/10.1186/ar3199.
[5] N. Dalbeth, L. Stamp, T. Merriman, Gout, Available from: Ebook Central:, Oxford University Press, Oxford, 2016 https://ebookcentral.proquest.com/lib/northwu-ebooks/reader.action?docID=4310761. (Accessed 15 March 2021).

[6] A.A. Negm, D.E. Furst, Nonsteroidal anti-inflammatory drugs, disease-modifying antirheumatic drugs, nonopioid analgesics & drugs used in gout, in: B.G. Katzung (Ed.), Basic & Clinical Pharmacology, McGrawHill Education, San Francisco, 2018, pp. 642–666.
[7] G. Ragab, M. Elshahaly, T. Bardin, Gout: an old disease in new perspective – a review, J. Adv. Res. 8 (5) (2017) 495–511, https://doi.org/10.1016/j.jare.2017.04.008. (Accessed 6 September 2022).
[8] B. Wells, J. Dipiro, T. Schwinghammer, C. Dipiro, Gout & hyperuriceamia, in: T. Schwinghammer (Ed.), Pharmacotherapy Handbook, seventh ed., McGraw-Hill, New York, 2009, pp. 1–8.
[9] D. Rossiter, M. Blockman, K. Barnes (Eds.), South African Medicines Formulary, thirteenth ed., South African Medical Association, Pretoria, 2020.
[10] A. Pineau, O. Guillard, B. Fauconneau, F. Favreau, M.-H. Marty, A. Gaudin, C. M. Vincent, A. Marrauls, J.-P. Marty, *In vitro* study of percutaneous absorption of aluminum from antiperspirants through human skin in the Franz™ diffusion cell, J. Inorg. Biochem. 110 (2012) 21–26, https://doi.org/10.1016/j.jinorgbio.2012.02.013. (Accessed 6 September 2022).
[11] M.N. Sithole, S. Marais, S.M. Maree, L.H. Du Plessis, J. Du Plessis, M. Gerber, Development and characterisation of nano-emulsions and nano-emulgels for transdermal delivery of statins, Expet Opin. Drug Deliv. 18 (6) (2021) 789–801, https://doi.org/10.1080/17425247.2021.1867533.
[12] T.N. Chinembiri, M. Gerber, L.H. Du Plessis, J.L. Du Preez, J.H. Hamman, J. Du Plessis, Topical delivery of *Withania somnifera* crude extracts in niosomes and solid lipid nanoparticles, Phcog. Mag. 13 (2017) S663–S671, https://doi.org/10.4103/pm.pm_489_16.
[13] C. Csongradi, J. Du Plessis, M.E. Aucamp, M. Gerber, Topical delivery of roxithromycin solid-state forms entrapped in vesicles, Eur. J. Pharm. Biopharm. 114 (2017) 96–107, https://doi.org/10.1016/j.ejpb.2017.01.006.
[14] L. Van Zyl, J. Du Preez, M. Gerber, J. Du Plessis, J. Viljoen, Essential fatty acids as transdermal penetration enhancers, J. Pharmaceut. Sci. 105 (2016) 188–193, https://doi.org/10.1016/j.xphs.2015.11.032.
[15] C. Burger, M. Aucamp, J. Du Preez, R.K. Haynes, A. Ngwane, J. Du Plessis, M. Gerber, Formulation of natural oil nano-emulsions for the topical delivery of clofazimine, artemisone and decoquinate, Pharmaceut. Res. 35 (10) (2018) 186, https://doi.org/10.1007/s11095-018-2471-9.
[16] J.-C. Tsai, S.-A. Chuang, M.-Y. Hsu, H.-M. Sheu, Distribution of salicylic acid in human stratum corneum following topical application in vivo: a comparison of six different formulations, Int. J. Pharm. 188 (2) (1999) 145–153, https://doi.org/10.1016/S0378-5173(99)00217-3. (Accessed 26 July 2022).
[17] M.A. Pellett, M.S. Roberts, J. Hadgraft, Supersaturated solutions evaluated with an in vitro stratum corneum tape stripping technique, Int. J. Pharm. 151 (1) (1997) 91–98, https://doi.org/10.1016/s0378-5173(97)04897-7.
[18] K. Niska, E. Zielinska, M.W. Radomski, I. Inkielewicz-Stepniak, Metal nanoparticles in dermatology and cosmetology: interactions with human skin cells, Chem. Biol. Interact. 295 (2018) 38–51, https://doi.org/10.1016/j.cbi.2017.06.018. (Accessed 1 September 2022).
[19] A. Jaeger, D.G. Weiss, L. Jonas, R. Kriehuber, Oxidative stress-induced cytotoxic and genotoxic effects of nano-sized titanium dioxide particles in human HaCaT keratinocytes, Toxicology 296 (1) (2012) 27–36, https://doi.org/10.1016/j.tox.2012.02.016.
[20] S.H. Lee, H.R. Lee, Y.-R. Kim, M.-K. Kim, Toxic response of zinc oxide nanoparticles in human epidermal keratinocyte HaCaT cells, Toxicol. Environ. Health Sci. 4 (1) (2012) 14–18, https://doi.org/10.1007/s13530-012-0112-y.
[21] T. Groth, B. Seifert, G.N. Malsch, W. Albrecht, D. Paul, A. Kostadinova, A. Krasteva, G. Altankov, Interaction of human skin fibroblasts with moderate wettable polyacrylonitrile-copolymer membranes, J. Biomed. Mater. Res. 61 (2) (2002) 290–300, https://doi.org/10.1002/jbm.10191.
[22] A. Ribeiro, T. Matamá, C.F. Cruz, A.C. Gomes, A.M. Cavaco-Paulo, Potential of human γD-crystallin for hair damage repair: insights into the mechanical properties and biocompatibility, Int. J. Cosmet. Sci. 35 (5) (2013) 458–466, https://doi.org/10.1111/ics.12065.
[23] F. Albano, A. Arcucci, G. Granato, S. Romano, S. Montagnani, E. De Vendittis, M. R. Ruocco, Markers of mitochondrial dysfunction during the diclofenac-induced apoptosis in melanoma cell lines, Biochimie 95 (4) (2013) 934–945, https://doi.org/10.1016/j.biochi.2012.12.012. (Accessed 9 July 2022).
[24] B. Iovine, M.L. Iannella, F. Gasparri, G. Monfrecola, M.A. Bevilacqua, Synergic effect of genistein and daidzein on UVB-induced DNA damage: an effective photoprotective combination, J. Biomed. Biotechnol. 2011 (2011) 1–8, https://doi.org/10.1155/2011/692846.
[25] M. Brown, C. Wallace, C. Anamelechi, E. Clermont, W. Reichert, G. Truskey, The use of mild trypsinization conditions in the detachment of endothelial cells to promote subsequent endothelialization on synthetic surfaces, Biomaterials 28 (27) (2007) 3928–3935, https://doi.org/10.1016/j.biomaterials.2007.05.009.
[26] J.V. Olsen, S.-E. Ong, M. Mann, Trypsin cleaves exclusively c-terminal to arginine and lysine residues, Mol. Cell. Proteomics 3 (6) (2004) 608–614, https://doi.org/10.1074/mcp.t400003-mcp200.
[27] A. Dwivedi, A. Mazumder, L.T. Fox, A. Brümmer, M. Gerber, J.L. du Preez, R. K. Haynes, J. du Plessis, In vitro skin permeation of artemisone and its nano-vesicular formulations, Int. J. Pharm. 503 (1) (2016) 1–7, https://doi.org/10.1016/j.ijpharm.2016.02.041. (Accessed 8 October 2016).
[28] A. Naik, Y.N. Kalia, R.H. Guy, Transdermal drug delivery: overcoming the skin's barrier function, Pharmaceut. Sci. Technol. Today 3 (9) (2000) 318–326, https://doi.org/10.1016/s1461-5347(00)00295-9.
[29] P.A. Makoni, J. Ranchhod, K. WaKasongo, S.M. Khamanga, R.B. Walker, The use of quantitative analysis and Hansen solubility parameter predictions for the selection of excipients for lipid nanocarriers to be loaded with water soluble and insoluble compounds, Saudi Pharmaceut. J. 28 (3) (2020) 308–315, https://doi.org/10.1016/j.jsps.2020.01.010. (Accessed 21 August 2022).
[30] T.D. Bergazin, N. Tielker, Y. Zhang, J. Mao, M.R. Gunner, K. Francisco, Evaluation of log P, pKa, and log D predictions from the SAMPL7 blind challenge, J. Comput. Aided Mol. Des. 35 (7) (2021) 771–802, 0.1007/s10822-021-00397-3.
[31] U.S. Environmental Protection Agency, CompTox Chemicals Dashboard: Colchicine, 2021. https://comptox.epa.gov/dashboard/dsstoxdb/results?search=DTXSID5024845#properties. (Accessed 22 May 2021).
[32] D. N'Da, Prodrug strategies for enhancing the percutaneous absorption of drugs, Molecules 19 (12) (2014) 20780–20807, https://doi.org/10.3390/molecules191220780.
[33] M.H. Lee, G.H. Shin, H.J. Park, Solid lipid nanoparticles loaded thermoresponsive pluronic-xanthan gum hydrogel as a transdermal delivery system, J. Appl. Polym. Sci. 135 (11) (2018) 1–10, https://doi.org/10.1002/app.46004.
[34] I. Gutowski, The Effects of pH and Concentration on the Rheology of Carbopol Gels, Canada: Simon Fraser University, 2008 (Thesis – PhD), https://core.ac.uk/download/pdf/56375548.pdf. (Accessed 27 April 2022).
[35] J. Alemán, A.V. Chadwick, J. He, M. Hess, K. Horie, R.G. Jones, P. Kratochvíl, I. Meisel, I. Mita, G. Moad, S. Penczek, G. Moad, Definitions of terms relating to the structure and processing of sols, gels, networks, and inorganic-organic hybrid materials (IUPAC Recommendations 2007), Pure Appl. Chem. 79 (10) (2007) 1801–1829. https://www.degruyter.com/document/doi/10.1351/pac200779101801/html. (Accessed 7 September 2022).
[36] J. Li, D.J. Mooney, Designing hydrogels for controlled drug delivery, Nat. Rev. Mater. 1 (12) (2016) 1–38, https://doi.org/10.1038/natrevmats.2016.71.
[37] C.S.A.D. Lima, T.S. Balogh, J.P.R.O. Varca, G.H.C. Varca, A.B. Lugão, L. A. Camacho-Cruz, E. Bucio, S.S. Kadlubowski, An updated review of macro, micro, and nanostructured hydrogels for biomedical and pharmaceutical applications, Pharmaceutics 12 (2020) 1–28, https://doi.org/10.3390/pharmaceutics12100970.
[38] P. Schmiedel, W. Von Rybinski, Applied theory of surfactants, Available from: Google Books:, in: R.J. Farn (Ed.), Chemistry and Technology of Surfactants, Blackwell Publishing Limited, Oxford, 2006, pp. 46–88 https://books.google.co.za/books?hl=en&lr=&id=CCn81pnPrgwC&oi=fnd&pg=PA1&dq=surfactants+and+emulsifiers&ots=cMIr-qipgP&sig=ql0fKs2zPCdPlAoPuWcTsJAnyBA#v=onepage&q=surfactant&f=false. (Accessed 11 May 2022).
[39] D. Ramadon, A.W. Goldie, E. Anwar, Novel transdermal ethosomal gel containing green tea (Camellia sinensis L. Kuntze) leaves extract: formulation and in vitro penetration study, J. Young Pharm. 9 (3) (2017) 336–340. https://pdfs.semanticscholar.org/4fad/7302d1255725424c1cee4c79f89c31ae4ec0.pdf. (Accessed 12 May 2022).
[40] G. Coneac, V. Vlaia, I. Olariu, A.M. Muț, D.F. Anghel, C. Ilie, C. Popoiu, D. Lupuleasa, L. Vlaia, Development and evaluation of new microemulsion-based hydrogel formulations for topical delivery of fluconazole, Am. Associat.Pharm. Sci. Pharm.Sci.Tech. 16 (4) (2015) 889–904, https://doi.org/10.1208/s12249-014-0275-8.
[41] S.M.T. Gharibzahedi, S. Mohammadnabi, Effect of novel bioactive edible coatings based on jujube gum and nettle oil-loaded nanoemulsions on the shelf life of Beluga sturgeon fillets, Int. J. Biol. Macromol. 95 (2017) 769–777, https://doi.org/10.1016/j.ijbiomac.2016.11.119. (Accessed 6 June 2022).
[42] M.I. Mohamed, A.A. Abdelbary, S.M. Kandil, T.M. Mahmoud, Preparation and evaluation of optimized zolmitriptan niosomal emulgel, Drug Dev. Ind. Pharm. 45 (7) (2019) 1157–1167, 0.1080/03639045.2019.1601737.
[43] C.T. Ueda, V.P. Shah, K. Derdzinski, G. Ewing, G. Flynn, H. Maibach, M. Marques, H. Rytting, S. Shaw, K. Thakker, A. Yacobi, Topical and transdermal drug products, Pharmacopeial Forum 35 (3) (2009) 750–764. https://oarklibrary.com/file/2/ab583750-8928-4952-ba9a-1fa6490e21b0/3b2ed1d9-2635-4f8c-b92e-f390e05f633e.pdf. (Accessed 5 October 2022).
[44] Lubrizol Corporation, Viscosity of Carbopol®* polymers in aqueous systems (technical data sheet: TDS-730). https://www.lubrizol.com/-/media/Lubrizol/Health/TDS/TDS-730_Viscosity_Carbopol_in_Aqueous-Systems.pdf, 2010. (Accessed 29 September 2022).
[45] V. Klang, J.C. Schwarz, C. Valenta, Nanoemulsions in dermal drug delivery, in: N. Dragicevic, H.I. Maibach (Eds.), Percutaneous Penetration Enhancers, Chemical Methods in Penetration Enhancement: Drug Manipulation Strategies and Vehicle Effects, Springer, Berlin, 2015, pp. 255–266, https://doi.org/10.1007/978-3-662-45013-0_18.
[46] S. Choudhury, S. Dasgupta, D.K. Patel, Y.R. Ramani, S.K. Ghosh, B. Mazumder, Nanoemulsion as a carrier for topical delivery of aceclofenac, in: Giri, et al. (Eds.), Advanced Nanomaterials and Nanotechnology, Springer, Berlin, 2013, pp. 1–19, https://doi.org/10.1007/978-3-642-34216-5_1.
[47] C. Solans, P. Izquierdo, J. Nolla, N. Azemar, M. Garciacelma, Nano-emulsions, Curr. Opin. Colloid Interface Sci. 10 (2005) 102–110, https://doi.org/10.1016/j.cocis.2005.06.004.
[48] N. Singh, S.M. Verma, S.K. Singh, P.R.P. Verma, M.N. Ahsan, Antibacterial activity of cationised and non-cationised placebo lipidic nanoemulsion using transmission electron microscopy, J. Exp. Nanosci. 10 (4) (2015) 299–309, https://doi.org/10.1080/17458080.2013.830199.
[49] M.Y. Koroleva, E.V. Yurtov, Nanoemulsions: the properties, methods of preparation and promising applications, Russ. Chem. Rev. 81 (1) (2012) 21–43, https://doi.org/10.1070/rc2012v081n01abeh004219.
[50] M. Nasr, H. Younes, R.S. Abdel-Rashid, Formulation and evaluation of cubosomes containing colchicine for transdermal delivery, Drug Deliv. Translat.Res. 10 (5) (2020) 1302–1313, https://doi.org/10.1007/s13346-020-00785-6.
[51] C.B. Thompson, Descriptive data analysis, Air Med. J. 28 (2) (2009) 56–59, https://doi.org/10.1016/j.amj.2008.12.001. (Accessed 1 October 2022).

[52] Y. Zhang, W. Ng, J. Hu, S.S. Mussa, Y. Ge, H. Xu, Formulation and *in vitro* stability evaluation of ethosomal carbomer hydrogel for transdermal vaccine delivery, Colloids Surf. B Biointerfaces 163 (2018) 184–191, https://doi.org/10.1016/j.colsurfb.2017.12.031. (Accessed 8 October 2022).
[53] K. Kathe, H. Kathpalia, Film forming systems for topical and transdermal drug delivery, Asian J. Pharm. Sci. 12 (6) (2017) 1–11, https://doi.org/10.1016/j.ajps.2017.07.004.
[54] S. Md, N.A. Alhakamy, H.M. Aldawsari, S. Kotta, J. Ahmad, S. Akhter, M.S. Alam, M.A. Khan, Z. Awan, P.M. Sivakumar, Improved analgesic and anti-inflammatory effect of diclofenac sodium by topical nanoemulgel: formulation development *in vitro* and *in vivo* studies, J. Chem. 2020 (2020) 1–10, https://doi.org/10.1155/2020/4071818.
[55] B. Hajjar, K.-I. Zier, N. Khalid, S. Azarmi, R. Löbenberg, Evaluation of a microemulsion-based gel formulation for topical drug delivery of diclofenac sodium, J. Pharm.Investigat. 48 (3) (2018) 351–362, https://doi.org/10.1007/s40005-017-0327-7.
[56] T. Dahiru, P-Value, a true test of statistical significance, a cautionary note, Ann. Ib. Postgrad. Med. 6 (1) (2011) 21–26, https://doi.org/10.4314/aipm.v6i1.64038.
[57] M.R. Abdulbaqi, N. Rajab, Apixaban ultrafine O/W nano emulsion transdermal drug delivery system: formulation, *in vitro* and *ex vivo* characterization, Sys. Rev. Pharm. 11 (2020) 82–94. https://www.researchgate.net/profile/Mustafa-R-Abdulbaqi/publication/349253871. (Accessed 7 October 2022). Apixaban_Ultrafine_OW_Nano_Emulsion_Transdermal_Drug_Delivery_System_Formulation_In_Vitro_and_Ex_Vivo_Characterization/links/603965c2299bf1cc26f41397/Apixaban-Ultrafine-O-W-Nano-Emulsion-Transdermal-Drug-Delivery-System-Formulation-In-Vitro-and-Ex-Vivo-Characterization.pdf.
[58] U. Syamala, Development & optimization of allyl amine antifungal nanoemulgel using $2^3$ factorial design: for the treatment of tinea pedis, Eur. Sci. J. (2013). https://www.researchgate.net/profile/Marcin-Jewdokimow/publication/259994368_Creativity_at_School_Conclusions_from_Polish_Study/links/02e7e52ef780b21480000000/Creativity-at-School-Conclusions-from-Polish-Study.pdf#page=609. (Accessed 7 October 2022).
[59] M. Schäfer-Korting, W. Mehnert, H.-C. Korting, Lipid nanoparticles for improved topical application of drugs for skin diseases, Adv. Drug Deliv. Rev. 59 (6) (2007) 427–443, https://doi.org/10.1016/j.addr.2007.04.006. (Accessed 10 November 2022).
[60] C. Burger, M. Gerber, J.L. du Preez, J. du Plessis, Optimised transdermal delivery of pravastatin, Int. J. Pharm. 496 (2) (2015) 518–525, https://doi.org/10.1016/j.ijpharm.2015.10.034. (Accessed 11 November 2022).
[61] A.M. Barbero, H.F. Frasch, Effect of stratum corneum heterogeneity, anisotropy, asymmetry and follicular pathway on transdermal penetration, J. Contr. Release 260 (2017) 234–246, https://doi.org/10.1016/j.jconrel.2017.05.034.
[62] H.A.E. Benson, Skin structure, function, and permeation, Available from: Prorequest ebookcentral:, in: H.A.E. Benson, A.C. Watkinson (Eds.), Transdermal and Topical Drug Delivery, 2012, pp. 3–22 https://ebookcentral.proquest.com/lib/northwu-ebooks/reader.action?docID=693203. (Accessed 24 February 2021).
[63] E. Haltner-Ukomadu, M. Sacha, A. Richter, K. Hussein, Hydrogel increases diclofenac skin permeation and absorption, Biopharm Drug Dispos. 40 (7) (2019) 217–224, https://doi.org/10.1002/bdd.2194.
[64] B. Kim, H.-E. Cho, S.H. Moon, H.-J. Ahn, S. Bae, H.-D. Cho, S. An, Transdermal delivery systems in cosmetics, Biomed.Dermatol. 4 (10) (2020) 1–12, https://doi.org/10.1186/s41702-020-0058-7.
[65] A. Ahsan, W.-X. Tian, M.A. Farooq, D.H. Khan, An overview of hydrogels and their role in transdermal drug delivery, Int.J.Polym.Mater. Polym. Biomater. 70 (8) (2021) 574–584, https://doi.org/10.1080/00914037.2020.1740989.
[66] Morsy, L. Abdel, Venugopala Nair, Elsewedy Ahmed, Shehata, Preparation and evaluation of atorvastatin-loaded nanoemulgel on wound-healing efficacy, Pharmaceutics 11 (11) (2019) 609, https://doi.org/10.3390/pharmaceutics11110609.
[67] C.L. Winek, W.W. Wahba, C.L. Winek, T.W. Balzer, Drug and chemical blood-level data 2001, Forensic Sci. Int. 122 (2) (2001) 107–123, https://doi.org/10.1016/S0379-0738(01)00483-2. (Accessed 1 November 2022).
[68] K. Ng, Penetration enhancement of topical formulations, Pharmaceutics 10 (2) (2018) 1–3, https://doi.org/10.3390/pharmaceutics10020051.
[69] S. Lee, C. Woo, C.S. Ki, Pectin nanogel formation via thiol-norbornene photo-click chemistry for transcutaneous antigen delivery, J. Ind. Eng. Chem. 108 (2022) 159–169, https://doi.org/10.1016/j.jiec.2021.12.038. (Accessed 11 October 2022).
[70] R.R. Warner, K.J. Stone, Y.L. Boissy, Hydration disrupts human stratum corneum ultrastructure, J. Invest. Dermatol. 120 (2) (2003) 275–284, https://doi.org/10.1046/j.1523-1747.2003.12046.x. (Accessed 10 November 2022).
[71] A.C. Williams, B.W. Barry, Penetration enhancers, Adv. Drug Deliv. Rev. 64 (2012) 128–137, https://doi.org/10.1016/j.addr.2012.09.032.
[72] W.-R. Lee, S.-C. Shen, H.-H. Lai, C.-H. Hu, J.-Y. Fang, Transdermal drug delivery enhanced and controlled by erbium: YAG laser: a comparative study of lipophilic and hydrophilic drugs, J. Contr. Release 75 (1) (2001) 155–166, https://doi.org/10.1016/S0168-3659(01)00391-1. (Accessed 12 November 2022).
[73] H. Trommer, R.H.H. Neubert, Overcoming the stratum corneum: the modulation of skin penetration, Skin Pharmacol. Physiol. 19 (2) (2006) 106–121, https://doi.org/10.1159/000091978.
[74] J. Du Plessis, C. Ramachandran, N. Weiner, D. Muller, The influence of particle size of liposomes on the deposition of drug into skin, Int. J. Pharm. 103 (3) (1994) 277–282, https://doi.org/10.1016/0378-5173(94)90178-3.
[75] V.C. Jhawat, V. Saini, S. Kamboj, N. Maggon, Transdermal drug delivery systems: approaches and advancements in drug absorption through skin, Int. J. Pharmaceut. Sci. Rev. Res. 20 (1) (2013) 47–56. https://www.researchgate.net/profile/Vikas-Jhawat/publication/281891169. (Accessed 12 October 2022). Transdermal_Drug_Delivery_Systems_Approaches_and_Advancements_in_Drug_Absorption_through_Skin/links/560a4c4108ae4d86bb137040/Transdermal-Drug-Delivery-Systems-Approaches-and-Advancements-in-Drug-Absorption-through-Skin.pdf.
[76] S.A. Rashid, S. Bashir, H. Ullah, D.H. Khan, P.A. Shah, M.Z. Danish, M.H. Khan, S. Mahmood, M. Sohaib, M.M. Irfan, A. Amin, Development, characterization and optimization of methotrexate-olive oil nano-emulsion for topical application, Pak. J. Pharm. Sci. 34 (1) (2021) 205–215, https://doi.org/10.36721/PJPS.2021.34.1.SUP.205-215.1.
[77] A. Shahbaz, Development and optimization of nanoemulsion formulation for topical treatment of candidiasis. Turkish republic of northern Cyprus: near east university (thesis – master). http://docs.neu.edu.tr/library/7129855414.pdf, 2020. (Accessed 11 November 2022).
[78] J. Weyermann, D. Lochmann, A. Zimmer, A practical note on the use of cytotoxicity assays, Int. J. Pharm. 288 (2) (2005) 369–376, https://doi.org/10.1016/j.ijpharm.2004.09.018. (Accessed 14 July 2022).
[79] J. López-García, M. Lehocký, P. Humpolíček, P. Sáha, HaCaT keratinocytes response on antimicrobial atelocollagen substrates: extent of cytotoxicity, cell viability and proliferation, J. Funct. Biomater. 5 (2) (2014) 43–57, https://doi.org/10.3390/jfb5020043.
[80] B. Rawtal, T. Ayachit, D. Wasule, S. Sahasrabuddhe, N. Bajpai, Nanocosmeceuticals a boon to cosmetic industry, Res. J. 14 (2) (2018) 1–75. https://ladcollege.ac.in/wp-content/uploads/2022/01/Research-Journal-142-2018.pdf#page=15. (Accessed 13 November 2022).
[81] A. Otto, J. Du Plessis, J.W. Wiechers, Formulation effects of topical emulsions on transdermal and dermal delivery, Int. J. Cosmet. Sci. 31 (1) (2009) 1–19, https://doi.org/10.1111/j.1468-2494.2008.00467.x.